Synchronization and entrainment of metapopulations: A trade-off among time-induced heterogeneity, dispersal, and seasonal force

Ramesh Arumugam and Partha Sharathi Dutta*
Department of Mathematics, Indian Institute of Technology Ropar, Punjab-140 001, India

(Received 5 January 2018; revised manuscript received 7 February 2018; published 22 June 2018)

Demographic and environmental heterogeneities are prevalent across many natural systems. Earlier studies on metapopulation models have mostly considered heterogeneities either in the demographic parameters or in the interaction strength and topology between the spatially separated patches. In contrast, here we study the dynamics of a metapopulation model where each of the uncoupled patches has different periods of oscillations (period mismatch). We show different synchronization dynamics governed by both period mismatch and dispersal in neighboring patches. Indeed, we find both appearance and disappearance of phase synchronization, quasiperiodic oscillations, and period doubling of limit cycle. We also quantify the effect of seasonal variation (entrainment) and dispersal on species synchrony using phase-response curve and a synchrony measure, which thereof identify the influence of stochasticity on species persistence through trade-off mechanisms. Our results show that trade-offs among period mismatch, dispersal, and external force can drive entrained oscillations as well as asynchronous population dynamics that structure ecological communities.

DOI: 10.1103/PhysRevE.97.062217

I. INTRODUCTION

Oscillations are ubiquitous in many natural systems, which significantly governs the functioning of life through cyclic processes [1]. In various biological activities, such as cardiac oscillations [2], circadian rhythms [3], and seasonal succession [4], the characteristics of oscillations are inherently associated with their self-organization [5]. At the same time, various intrinsic and extrinsic factors are known to influence oscillations and can induce correlated or synchronized behavior in coupled systems. In spatial ecosystems, occurrence of such synchronous fluctuations in species abundance are widespread [6–9]. In fact, *metapopulation*, which is a population of spatially distributed populations that often are connected with dispersal [10], shows correlated fluctuations in species abundance with neighboring populations [11–13]. For example, Hanski [14,15] reviewed a long-term investigation on the Glanville fritillary butterfly (*Melitaea cinxia*), which shows synchronous behavior in a spatial network of 4000 dry meadows in Finland.

Most of the theoretical as well as empirical studies on population synchrony have indicated two major mechanisms behind its occurrence: The first one is *species dispersal* (migration) describing species spatial movement and the second one is exogenous factors, such as weather, noise, climatic variation, etc., known as the *Moran effect* [6,16]. Generally, species dispersal as a density-dependent process is considered to be a building block of spatial ecology [17]. To characterize the effects of dispersal in spatial ecosystems, various network topologies have been used and gained much attention in understanding community structure [18–22]. Subsequently, the other major factor promoting synchronized state is the influence of stochasticity in the form of climatic variations as a density-independent process [16,23,24]. Through the periodic climatic variations, often species abundance are entrained to the external forces (known as *entrainment*) [25]. Therefore, the combination of density-dependent process with dispersal and density-independent processes with external perturbations encompasses the synchronous states in species abundance. In majority of the studies on population synchrony, a general consensus is that synchronous populations always have *higher risk of extinction*, in contrast to asynchronous populations, which in turn *promotes species persistence* [18,26]. Hence, considering the current fast rate of species extinction following habitat fragmentation [27], it is important to understand the influence of local population dynamics in inducing the global synchronous dynamics of metapopulations.

Heterogeneous characteristics of local populations are widespread in most of the spatial ecosystems [17,28–30]. The variations in environmental conditions over space or time as environmental (extrinsic) heterogeneity are largely involved with synchronous processes in spatial ecosystems. In most of the previous studies, the combination of trophic interactions, dispersal, and external force has been studied in characterizing the metapopulation synchronization [10–12,18]. However, a little is known in terms of scale-dependent heterogeneity in habitat patches. Although heterogeneity is considered in diverse aspects, such as variation in intrinsic dynamics [31], its distribution in spatial pattern [32,33], frequency variation [13], different dispersal network structure [18], etc., the emphasis on heterogeneity is inevitably dependent on scale. The scale-dependent heterogeneity can affect the synchronous state in metapopulations. To address this, we introduce *heterogeneity* in terms of *timescale differences*, i.e., each uncoupled patch in a metapopulation model has distinct period of oscillations (*period mismatch*) and aim to probe the following questions: How are period mismatch, dispersal, and seasonal fluctuations associated with time-dependent

*Corresponding author: parthasharathi@iitrpr.ac.in

habitats in promoting the synchronous state? What are the mechanisms involved in entraining the ecological system to the seasonal force? What are the trade-offs between seasonality, stochasticity, and nonlinearity on metapopulation persistence?

In this paper, using a metapopulation model, we show that in the presence of *period mismatch* between *uncoupled patches*, the spatial system exhibits interesting dynamics, such as phase synchronization, period doubling of limit cycle, and quasiperiodic oscillations. We also find that the right balance between period mismatch and dispersal rate can induce perfect synchrony and stability by suppressing the oscillations into identical steady states, namely *amplitude death* (AD) [31]. Further, the suppressed oscillations are revived again through dispersal, which is known as *rhythmogenesis* [34]. Thereafter, by emphasizing the influence of periodic external force, we quantify the coherent behavior of species abundance to external force (known as *entrainment*) using two distinct mechanisms: the *phase-reduction approach* [35] and the *correlation of time series* [36]. Higher entrainment in metapopulation occurs for a certain set of model parameters. Subsequently, considering a regular network topology consisting of 100 patches, with stochasticity and periodic distributions in external force, the qualitative variation in synchronous behavior from a regular to an irregular pattern is quantified using the synchrony measure. The resulting trade-offs between time-induced heterogeneity, dispersal, and seasonal force can shape ecological communities by enhancing metapopulation persistence.

We organize the paper as follows: In Sec. II, we describe a spatially structured form of the Rosenzweig–MacArthur (RM) model [37], in which the interacting patches show heterogeneity in their oscillation period. In Sec. III, we study various collective dynamics through the interplay of heterogeneity and dispersal in the absence as well as the presence of external perturbations. Specifically, the environmental variation through different external forces with distinct characteristics is studied using phase-reduction method in Sec. III C. Subsequently, the effect of external force is determined by entrainment and a synchrony measure for a large network is quantified in terms of seasonal forcing and random variation in period mismatch. Finally, the key findings and their ecological relevance are discussed in Sec. IV.

II. SPATIALLY STRUCTURED ROSENZWEIG-MACARTHUR MODEL

We analyze a spatially structured form of the RM model [37] consisting of resource density (V_i) and consumer density (H_i) in each patch (here i is the patch index). The consumer–resource interactions within the patch and the movement of consumers among the patches are taken into account, we distinguish the characteristics of each patch by introducing heterogeneity in the form of distinct period of oscillations. If we exclude the period mismatch, the patches are identical and their intrinsic dynamics are determined by logistic resource growth and type-II functional response at consumer level. Subsequently, the movement of the consumers is considered as diffusive process among the spatially separated patches, which is accounted through a simple diffusive coupling. Hence, the spatial model of the resource (V_i) and the consumer (H_i) are defined as:

$$\frac{dV_i}{dt} = \frac{1}{p_i}\left[rV_i\left(1-\frac{V_i}{K}\right) - \frac{\alpha V_i}{V_i+B}H_i\right], \tag{1a}$$

$$\frac{dH_i}{dt} = \frac{1}{p_i}\left[\frac{\beta\alpha V_i}{V_i+B} - m\right]H_i + \epsilon(H_{i+1} - 2H_i + H_{i-1}), \tag{1b}$$

where $i = 1,2,\ldots,N$, with N as the total number of patches. The local parameters r and K denote the intrinsic growth rate and the carrying capacity of V_i, respectively. α and B represent the predation rate of H_i and the half saturation constant, respectively. β is the efficiency of H_i through predation and m is its natural mortality rate.

Further, p_i denotes a scaling parameter which initially turns out to be the oscillation period of the uncoupled ith patch without altering the amplitude of oscillation and assumes different values for distinct patches (i.e., $p_i \neq p_j$ for $i \neq j$). This makes each of the patches heterogeneous with mismatched periods of oscillations. Due to anthropogenic factors, habitats are fragmented in spatial ecosystems. This fragmentation leads to change in the quality of each patch for species survival. Indeed, the considered period of oscillation in our model determines the quality of each habitat with a change in time duration of individual life (i.e., species longevity) in each patch. Earlier it has been shown that habitat quality and species persistence can be determined by its oscillation period [38]. In fact, here the introduced heterogeneity in oscillation period alters important demographic (intrinsic) species parameters, such as the growth rate, the predation rate, and the mortality rate [39]. These traits are directly involved in varying the oscillation period. However, the carrying capacity and the half-saturation constant have indirect effect on species behavior and they are interrelated with the collective dynamics of the system. As already mentioned, when uncoupled as well as without heterogeneity, all patches are identical in their intrinsic dynamics and have period (say τ) for a specific set of parameter values. By introducing heterogeneity through the scaling parameter p_i, the period of ith patch becomes τp_i. At spatial level, the dispersal of consumer follows a nearest-neighbor coupling with a dispersal rate or an interaction strength as ϵ.

III. RESULTS

The uncoupled RM model [i.e., Eq. (1) with $\epsilon = 0$] can exhibit steady states as well as limit cycles. It has three possible equilibrium points: trivial $(V^*,H^*) = (0,0)$, resource only $(V^*,H^*) = (K,0)$, and coexistence of resource and consumer $(V^*,H^*) = (\frac{mB}{\alpha\beta-m}, \frac{Br\beta(K(\alpha\beta-m)-Bm)}{K(\alpha\beta-m)^2})$. The resource-consumer equilibrium point is stable if $\frac{B}{K} > \frac{\alpha\beta-m}{\alpha\beta+m}$. However, for variation in K, this equilibrium point loses its stability and gives rise to oscillatory dynamics through a supercritical Hopf bifurcation.

Here at first, by considering two patches (i.e., $N = 2$) in stable oscillatory state, the importance of the period mismatch on the dispersal characteristics of the coupled system are identified by calculating few time series. For simplicity, we rescale the local parameters such that initially each patch has period $\tau(=1)$ without the parameter p_i, whereas with p_i each uncoupled ith patch has mismatched period τp_i.

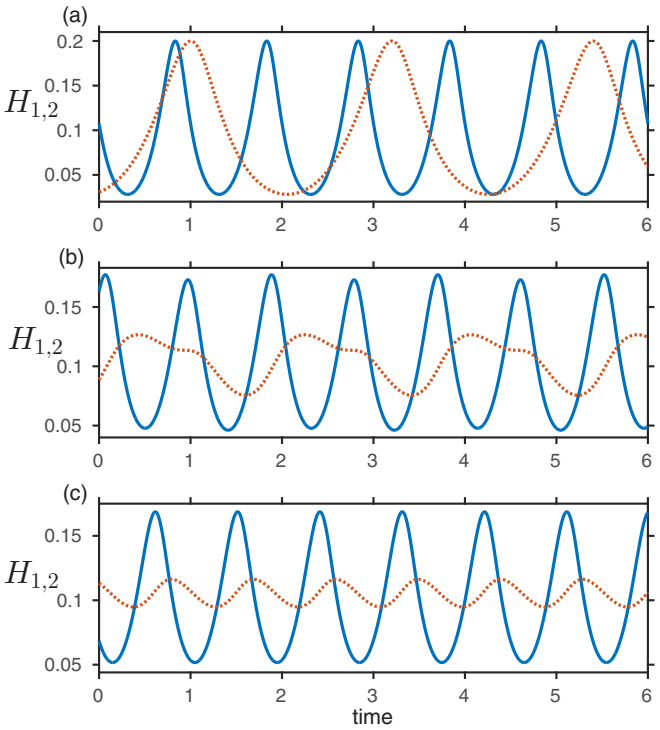

FIG. 1. Time series of the coupled RM model (1) for different values of the dispersal rate ϵ: (a) different periods of oscillation of H_i in two patches for $\epsilon = 0.0$, (b) stable period-2 cycles for $\epsilon = 0.8$, and (c) stable limit cycles with the same periods of oscillations for $\epsilon = 1$. Here the period mismatch in two patches are $p_1 = 1$ and $p_2 = 2.2$. The rescaled parameters are given by $r = 17.88$, $K = 0.5, \alpha = 35.76$, $\beta = 0.5$, $B = 0.16$, and $m = 7.152$.

Figure 1(a) shows different periods of oscillations of H_i (with $i = 1,2$) in different patches with $\epsilon = 0$. One can clearly distinguish between the mismatched periods of oscillations in each of the patches. However, variations in ϵ can induce qualitatively different asymptotic dynamics. For example, in another dispersal rate $\epsilon = 0.8$, we show a time series in which the oscillation has two different peaks. In fact, a period-2 cycles take place as shown in Fig. 1(b). Further variations in ϵ show phase-synchronized oscillations for $\epsilon = 1$ [see Fig. 1(c)], which indicates that populations are synchronized only in their relative phases, but not in their amplitude [40]. The qualitative dynamics of V_i are also similar. Given the presence of heterogeneity in each of the patches in terms of period mismatch and its interplay with dispersal rate, interesting complex dynamics occurs.

A. Quasiperiodicity and phase synchronization with variations in the period mismatch

For a wide range of heterogeneous periods, the collective dynamics of the model (1) are analyzed using the ratio between periods of oscillations in two patches. In particular, the ratio between the oscillation periods p_2 (of patch-2) and p_1 (of patch-1) is defined as

$$\text{Mismatch ratio: } p = \frac{p_2}{p_1}.$$

The dynamics of the model Eq. (1) with variations in p are analyzed using a one-parameter bifurcation diagram in Fig. 2 by depicting the maxima of the oscillation cycles of resource V_1 at two different values of dispersal rate (ϵ). In Fig. 2(a), we show the maxima of the limit cycle for varying period mismatch (p) with fixed dispersal rate $\epsilon = 0.85$. For increasing mismatch ratio p, the stable oscillations are changed to quasiperiodic oscillation through a torus bifurcation (TR1) at $p_{\text{TR1}} = 1.194$. In fact, for a range of p, the system exhibits quasiperiodic oscillations, which can also be identified through the Poincaré section [41]. Subsequently, for higher mismatch ratio, the torus size is decreased and further period doubling bifurcation (PD) of limit cycle takes place between $p = 2.193$ and $p = 2.217$, which is shown in the inset diagram of Fig. 2(a). Despite the fact that dynamically the coupled model has just diffusive coupling, the presence of heterogeneity in the oscillation periods exhibits period doubling and quasiperiodic dynamics. For higher mismatch ratio, again we have limit cycle oscillations. Similar qualitative dynamics holds in the consumer H_i also.

In another case, in Fig. 2(b), only stable limit cycle exists for continuous variation of the period mismatch ratio (p) with fixed $\epsilon = 1.2$. Here at low mismatch ratio (i.e., at $p =$

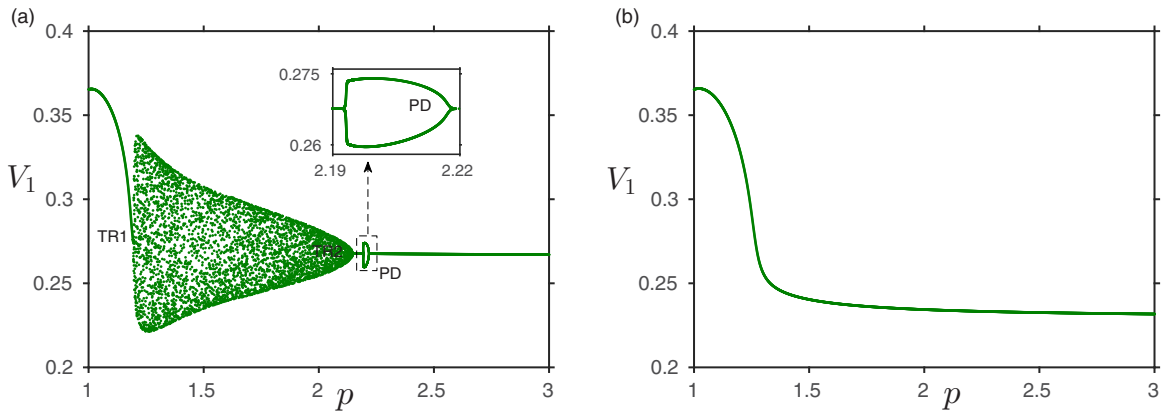

FIG. 2. Bifurcation diagrams of the metapopulation model (1) with variations in the mismatch ratio p. Local maximum value of V_1: (a) for fixed dispersal rate $\epsilon = 0.85$, and (b) for fixed dispersal rate $\epsilon = 1.2$. Here TR and PD denote torus and period-doubling bifurcations of limit cycles, respectively. Other parameters are given by $r = 17.88$, $K = 0.5$, $\alpha = 35.76$, $\beta = 0.5$, $B = 0.16$, and $m = 7.152$.

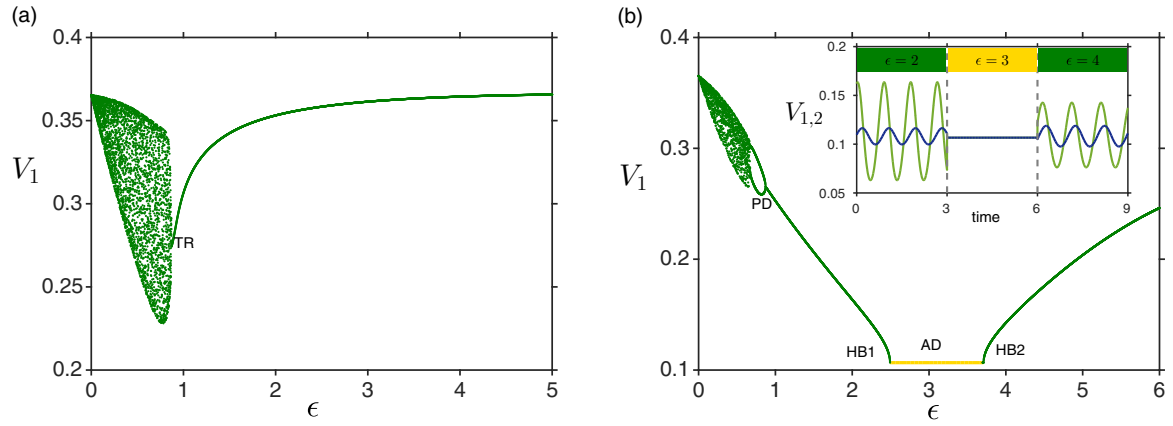

FIG. 3. Bifurcation diagrams of the metapopulation model (1) with variations in the dispersal rate ϵ. Local maximum value of V_1: (a) for fixed period mismatch ratio $p = 1.2$, and (b) for fixed period mismatch ratio $p = 2.2$. In (b), the yellow (light shaded) line (marked with AD) denotes stable steady states. Also PD, HB, and AD denote period-doubling bifurcation of limit cycle, Hopf bifurcation, and amplitude death, respectively. In the inset of (b), time series for three different values of ϵ are depicted. All the other parameters are the same as described in the caption of Fig. 2.

1, when both the patches are homogeneous with the same periods of oscillation) there is a decrease in the maxima of the limit cycle, whereas for higher mismatch ratio the maxima reaches a fixed value. Apart from these interesting dynamics, initially each patch oscillates with distinct phase, however due to strong enough coupling later they induce same phase with different amplitudes of oscillations. In fact, species from both the patch-1 and the patch-2 shows phase-synchronized oscillations [for exemplary time series, see Figs. 1(b) and 1(c)]. The existence of phase-synchronized behavior as well as stability of limit cycles can also be identified by Floquet multipliers (explained in the Appendix) [42]. A well-known example of phase synchronization in spatial ecological systems is the Canadian hare–lynx cycle, which follows a compact rhythm with an approximate oscillation period of 10 years [43]. From the ecological point view, synchronous oscillations are known to be detrimental for species persistence as it can enhance the risk of global extinction during the events of depression in population density and therefore potentially harmful for conservation biology [44]. In contrast, quasiperiodic and chaotic oscillations have less extinction risk and further constitutes increased persistence in the connected habitats [18,43].

B. Amplitude death with variations in the dispersal rate

As the species dispersal rate can vary with changes in climatic conditions, here the dynamics for changes in the dispersal rate ϵ are analyzed. For a continuous variation in ϵ with fixed period mismatch ratio p, the maxima of V_1 is shown in Fig. 3(a) using a one parameter bifurcation diagram. For a fixed $p = 1.2$, the coupled system exhibits quasiperiodic oscillation at low dispersal rate. However, for higher dispersal rate, the coupled system has stable limit cycle. Initially, the maxima of stable oscillation has increased for higher dispersal rate and further it saturates.

When $p = 2.2$, for different ranges of ϵ the model exhibits period doubling bifurcation, stable limit cycles, quasiperiodic oscillations and homogeneous steady states which are shown in Fig. 3(b). Here at first, quasiperiodic oscillation are shown at low dispersal rate. With an increase in the dispersal rate, quasiperiodicity leads to period doubling bifurcation of the limit cycle which then reduced to a stable period-one cycle at $\epsilon_{\mathrm{PD}} \approx 0.872$. Further increase in the ϵ leads to a decrease in the maxima of the limit cycle. Importantly, these phase-synchronized oscillations are transitioned to perfectly synchronized and homogeneous steady states (i.e., cessation of oscillations due to AD) through an interaction induced reverse supercritical Hopf bifurcation at $\epsilon_{\mathrm{HB1}} \approx 2.492$. Here, in Fig. 3(b) the yellow (light shaded) curve denotes homogeneous stable steady states. This supports species persistence as with stable steady states there is less risk of extinction of the population density if it is away from an extinction threshold [11]. With further increase in ϵ the suppressed oscillations are regenerated again through a supercritical Hopf bifurcation at $\epsilon_{\mathrm{HB2}} \approx 3.71$. Note that, the maxima of oscillation is again increasing after HB2 and shows phase synchronization. The complete change from phase-synchronized oscillations to perfectly synchronized steady state which further shifts to phase-synchronized oscillations are shown in the time series [see the inset diagram of Fig. 3(b)].

In our model, the introduced heterogeneity through period mismatch and the dispersal rate induces the synchronized behavior in combination of both stable oscillation and stable steady states. For a wide range of period mismatch ratio (p) and dispersal (ϵ), the region of stable oscillation and quasiperiodicity is shown in p–ϵ plane using two parameter bifurcation diagrams in Fig. 4(a). Here the parameter region of both dispersal and period mismatch where quasiperiodicity occurs is represented in shaded color region and also period doubling is denoted in another shaded color region. The TR curve marks the boundary between the limit cycle oscillation and the quasiperiodic oscillation. However, below the TR curve, only quasiperiodicity takes place, whereas above TR curve stable oscillation occurs. Also Figs. 2 and 3 are exhibiting particular cases of Fig. 4. There also exists a small region where period doubling bifurcation of limit cycle occurs (shown in inset diagrams). In the period doubling (PD) curve, the

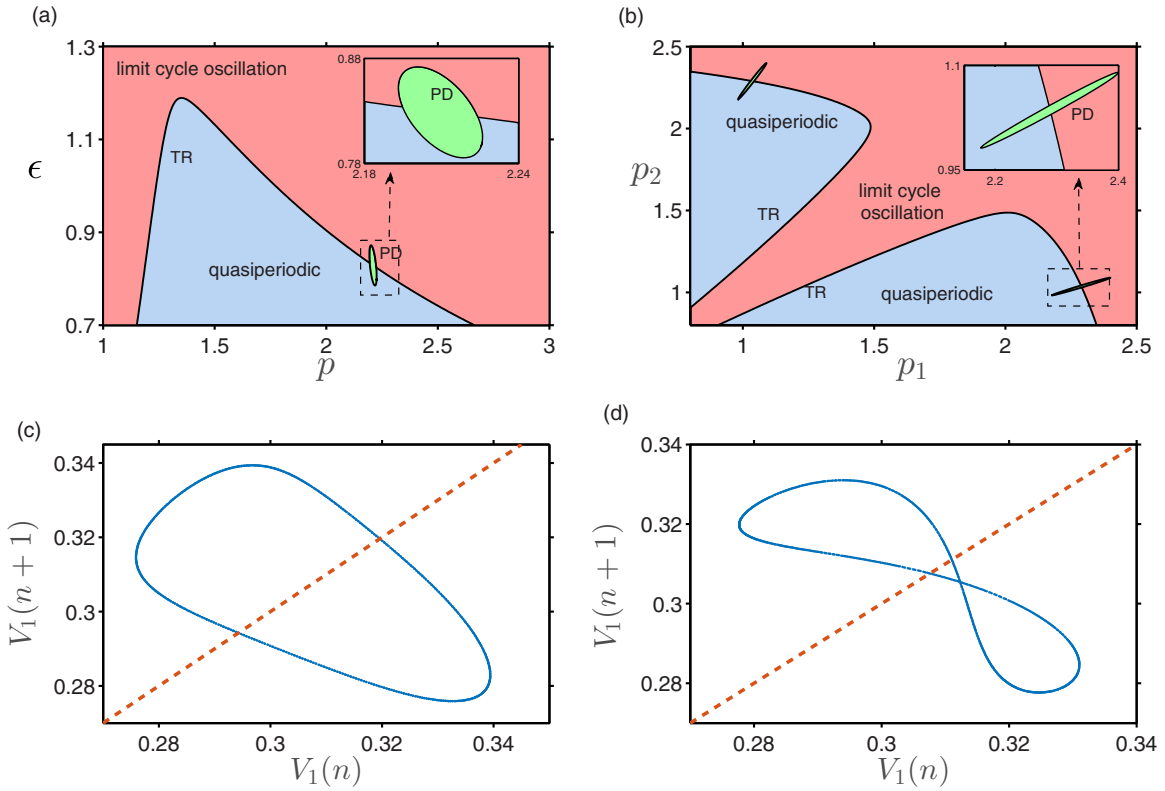

FIG. 4. Regions of limit cycle and quasiperiodic oscillations. Two parameter bifurcation diagrams: (a) in p–ϵ plane and (b) in p_1–p_2 plane for fixed dispersal rate $\epsilon = 0.8$. Here TR and PD denote torus bifurcation and period doubling bifurcation. Each color shaded region denotes existence of either limit cycle oscillations or quasiperiodic oscillations. (c) Quasiperiodicity through Poincaré section is represented in closed curve for $p = 1.6$ and $\epsilon = 0.5$; however, Poincaré section for a stable limit cycle is represented in dotted line. (d) Poincaré section for $p = 2$ and $\epsilon = 0.5$. All the other parameters are the same as described in the caption of Fig. 2.

closed circle represents starting and ending points of the period doubling bifurcation at a particular parameter value.

Instead of using the variations in mismatch ratio p, the actual dynamics of the model for changes in both p_1 and p_2 are shown in Fig. 4(b) for fixed ϵ. Since the considered spatial system with two patches has just simple diffusive coupling, the region where quasiperiodicity and stable oscillation occur is symmetrical. This is shown in p_1–p_2 plane. The occurrence of quasiperiodicity is identified through the Poincaré section by plotting peak-to-peak plot [41]. In Figs. 4(c) and 4(d), we have shown the peak-to-peak plot for two different values of p. From Fig. 4(c), the formation of closed curve determines that this is quasiperiodic oscillation with the same dynamical behavior, as shown in Fig. 4(d). The Poincaré section for stable limit cycles is represented in dotted line in both the Figs. 4(c) and 4(d).

C. Effect of periodic external force and entrainability of oscillations

As an extrinsic factor, often seasonal forcing strongly influences the species abundance of spatially distributed habitats [45]. In particular, the Moran effect is considered as one of the major mechanisms responsible for generating population synchrony under natural and laboratory conditions [46,47]. Moreover, perfect synchrony and phase synchrony also arise in spatial ecological system under the influence of environment [48,49]. By considering these characteristics, here we analyze the model Eq. (1) in the presence of a periodic external force as an extrinsic disturbance. At first, in the absence of external force, the coupled system Eq. (1) can be written as

$$\frac{d\mathbf{z}}{dt} = F(\mathbf{z}), \tag{2}$$

where $\mathbf{z} = [V_1\ H_1\ V_2\ H_2]^T$ and $F(\mathbf{z})$ is a vector derived from the right hand side of model Eq. (1). Applying the time-dependent external force $G(\omega t)$ with the strength ξ and angular frequency ω in the resource dynamics V_i, the Eq. (2) becomes

$$\frac{d\mathbf{z}}{dt} = F(\mathbf{z}) + \xi \mathbf{E} G(\omega t), \tag{3}$$

where $\mathbf{E} = [1\ 0\ 1\ 0]^T$ determines the assumption that only resource variables (V_i) are influenced by the external force. At primary level, the abundance of resource V_i is significantly affected by this seasonal forcing [50]. However, the consumer H_i is indirectly influenced by the seasonal force due to the consumer–resource interactions. To ensure periodic characteristics of the external force, a sinusoidal function is used as the seasonal force [50–52]:

$$G(\omega t) = a + b \sin(\omega t),$$

where a and b represent mean and amplitude of the sinusoidal external force.

1. Phase reduction for a perturbed limit cycle oscillator

The time-varying perturbations in the form of external force $G(\omega t)$ change the autonomous system [Eq. (1)] to a nonautonomous system [Eq. (3)]. In general, to elucidate the influence of external perturbations on the properties of coupled oscillators and their synchronization, often the phase-response curve (PRC) has been used which measures the response to perturbations at each phase of a limit cycle [53]. Using phase-reduction approach, the four-dimensional system Eq. (2), which exhibits a limit cycle oscillation, can be reduced to a one-dimensional phase equation with a phase variable ϕ [13,35]. In the absence of external force, a limit cycle oscillation can be described by the phase variable $\phi \in [0,2\pi]$ as

$$\frac{d\phi}{dt} = \Omega, \tag{4}$$

where Ω is the angular frequency of the limit cycle with period τ (i.e., $\Omega = 2\pi/\tau$). In the presence of external force $G(\omega t)$, the phase equation reads

$$\frac{d\phi}{dt} = \Omega + \xi\mathcal{Z}(\phi)\cdot G(\omega t). \tag{5}$$

Here dot $(\cdot)$ represents the dot product and $\mathcal{Z}(\phi)$ denotes the PRC, which describes the relationship between the perturbations and their response at each phase over a complete cycle [54], defined as

$$\mathcal{Z}(\hat{\phi}) = \nabla\phi(\mathbf{z})|_{\mathbf{z}=\mathbf{z}_0(\hat{\phi})},$$

where $\mathbf{z}_0(\hat{\phi})$ represents a point on the limit cycle at phase $\hat{\phi}$. By perturbing the system, the time taken to regain its original stable oscillation is represented in PRC. In other words, perturbations at each phase could cause the phase shift either lengthening or shortening the period. Positive phase shift in PRC indicates the phase advance, whereas negative phase shift indicates the phase delay induced by perturbation. Here, the PRC is computed using adjoint method. By considering a stable limit cycle, the PRC is computed numerically backward in time using Malkin's approach with the following adjoint equation [54–56]:

$$\frac{d\mathcal{Z}(t)}{dt} = -\{DF(\mathbf{z}_0(t))\}^{\top}\mathcal{Z}(t), \tag{6}$$

with

$$\mathcal{Z}(t)\cdot F(\mathbf{z}_0(t)) = \Omega,$$

where $DF(\mathbf{z}_0(t))$ is the Jacobian matrix of $F(\mathbf{z})$ around a stable periodic solution $\mathbf{z}_0(t)$ with period τ.

As the coupled system exhibits stable periodic dynamics at different dispersal rate and period mismatch, here we compute iPRC numerically where iPRC stands for infinitesimal PRC, which measures the effect of infinitesimally small

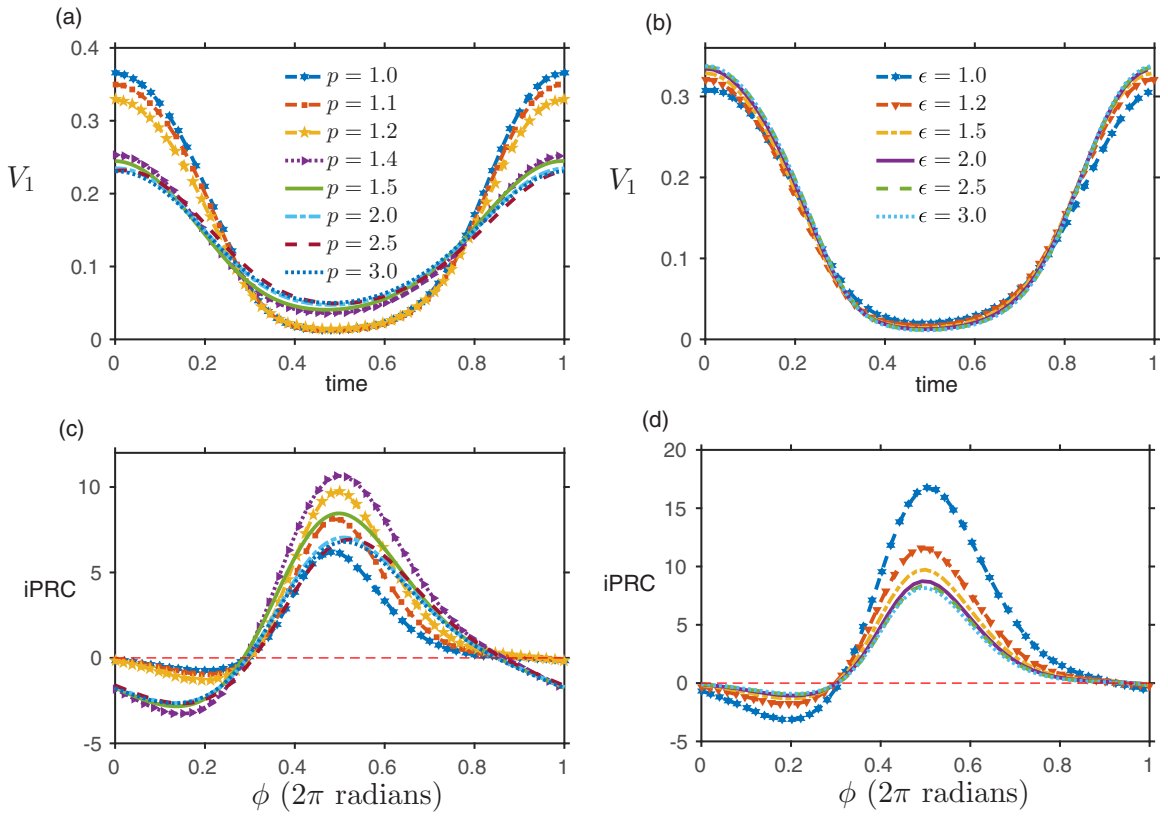

FIG. 5. Time series and phase-response curve: (a) At different mismatch ratio p, time series of a complete cycle in which period is rescaled to 1, and (c) phase-response curve of each time series of (a) with fixed $\epsilon = 1.5$. Here positive values of iPRC denote phase advance, whereas the negative values denote phase delay. (b) At each dispersal rate, time series of one complete cycle, and (d) its corresponding phase-response curves for each dispersal rate with fixed period mismatch ratio $p = 1.2$. All the other parameters are the same as described in the caption of Fig. 2.

perturbations on limit cycle. The time series of stable oscillation (i.e., one complete stable cycle) and its corresponding PRC over a cycle are shown in Fig. 5 for different values of p and ϵ. At low mismatch ratio p, the variation in the amplitude of the stable limit cycle oscillation is quite large, i.e., more than that for the higher mismatch ratio p [shown in Fig. 5(a)]. Also, the variations in the PRC with period mismatch ($p \neq 1$) and without period mismatch ($p = 1$) are shown in Fig. 5(c) for $\epsilon = 1.5$. The phases over a cycle are given along the x axis and the resulting phase shift after perturbation at each phase is along the y axis. Here the large region of positive phase shift indicates the phase advance induced by external perturbations. In fact, it is evident from Fig. 5 that at low abundance of species, the perturbation causes phase advance. Similarly, the time series and corresponding PRC at different dispersal rate (ϵ) for the fixed mismatch ratio (p) are shown in Figs. 5(b) and 5(d), respectively. With an increase in the dispersal rate, a small change in amplitude takes place, but higher variation emerges in the corresponding PRC. Hence, the combination of period mismatch and dispersal rate has strong impact on species density, particularly when a small perturbation takes place at low density. The computed PRC will be used in the next section to find the effect of the external force.

2. *Entrainment due to extrinsic disturbances in the presence of period mismatch*

Often ecological systems show synchronous behavior in response to external periodic signal, also known as entrainment [25,57]. Understanding the effect of seasonal forcing on heterogeneous ecological models is a key concern for ecosystem persistence [58]. Due to the interactions between two oscillating objects, the coherent behavior is enhanced through phase locking. Since the PRC determines the response of perturbations in the oscillating system, the computed PRC is also used to study the entrainment of the coupled system to the sinusoidal external force $G(\omega t)$. By using change of variable $\psi = \phi - \omega t$ in Eq. (5), we have

$$\frac{d\psi}{dt} = \Delta\Omega + \xi\Theta(\psi), \tag{7}$$

with $\Delta\Omega = \Omega - \omega$ and

$$\Theta(\psi) = \frac{1}{2\pi}\int_0^{2\pi} \mathcal{Z}(\psi+\theta)\cdot G(\theta)d\theta. \tag{8}$$

At each phase ψ, this integral [Eq. (8)] is evaluated numerically by time-averaging over the interval 0 to 2π. Importantly, the computed PRC and external force determine the range in which the coherent behavior holds. The coupled system can be synchronized for the sinusoidal external forces frequency if

$$\xi\Theta_{\min} + \Omega < \omega < \xi\Theta_{\max} + \Omega, \tag{9}$$

with

$$\Theta_{\min} = \min_{\psi}\Theta(\psi), \quad \text{and} \quad \Theta_{\max} = \max_{\psi}\Theta(\psi).$$

Entrainment of the coupled system requires that the external force frequency has to match reasonably with system's frequency. In particular, the range in which the system frequency can be synchronous with the seasonal force is determined by Arnold tongue (i.e., synchronization region) using $\xi(\Theta_{\max} - \Theta_{\min})$. The entrainability ($W$) is defined as

$$W = \Theta_{\max} - \Theta_{\min}, \tag{10}$$

which is ξ-independent.

We calculate the entrainment value [Eq. (10)] at each period mismatch ratio p using the PRC and sinusoidal external force $\sin(\omega t)$ with $\omega = 1$. For $\epsilon = 1.5$, in Fig. 6 we present the period τ of the coupled system Eq. (2) together with entrainability W using the dual axis (right y axis for τ and left y axis for W). We see that the period τ is influenced by changes in p. Initially the period is 1 at $p = 1$ and then around $p \approx 1.172$ it decays but finally stays close to 0.89. Relatively, the entrainability is enhanced for a certain range of heterogeneity due to mismatched period. In spite of having fixed period in external force (i.e., $\omega = 1$), higher entrainability emerges at various period mismatch ratio. This provides the strong support of considering habitat heterogeneity so that populations are entrained to seasonal variations. However, higher heterogeneity results in decreasing entrainability since the frequency of external force does not match with system's frequency.

D. Measure of synchrony in a metapopulation with 100 patches

In ecological systems, species abundances of spatially separated habitats are generally influenced by environmental forces and often exhibit correlated fluctuations [59–61]. It is also interesting to know how strongly they are correlated. Here, by considering external periodic forcing $G(\omega t)$ in a relatively large network ($N = 100$) of heterogeneous patches connected through simple diffusive coupling, we quantify the amount of synchronization by using a synchrony measure. First, in the network of 100 heterogeneous patches, the mismatch parameter p_i of each ith patch ($i = 1, \ldots, N$) is chosen randomly in such a way that the periodicity has mean 1 and standard deviation σ. Second, the effect of external force $G(\omega t)$ on the network synchronization is measured at different levels of forcing strength (ξ) for various standard deviation (σ).

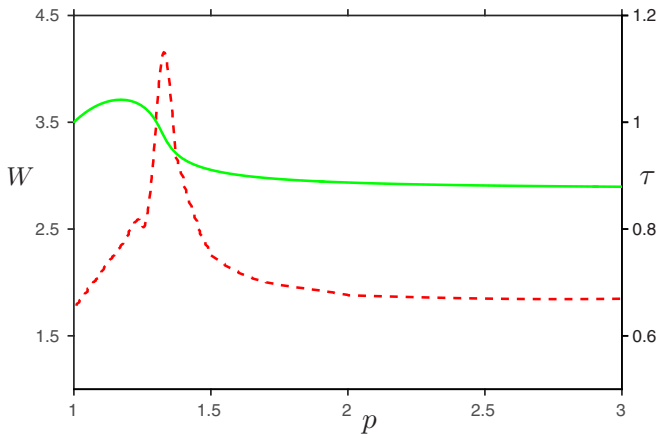

FIG. 6. Entrainment and period of oscillation for $\epsilon = 1.5$: At each period mismatch ratio (p), the entrainability (W) and the period of oscillations (τ) are shown in red (dashed curve) and green (solid curve), respectively, using dual axes. For the periodic external force, we use $a = 0$, $b = 1$, and $\omega = 1$. All the other parameters are the same as described in the caption of Fig. 2.

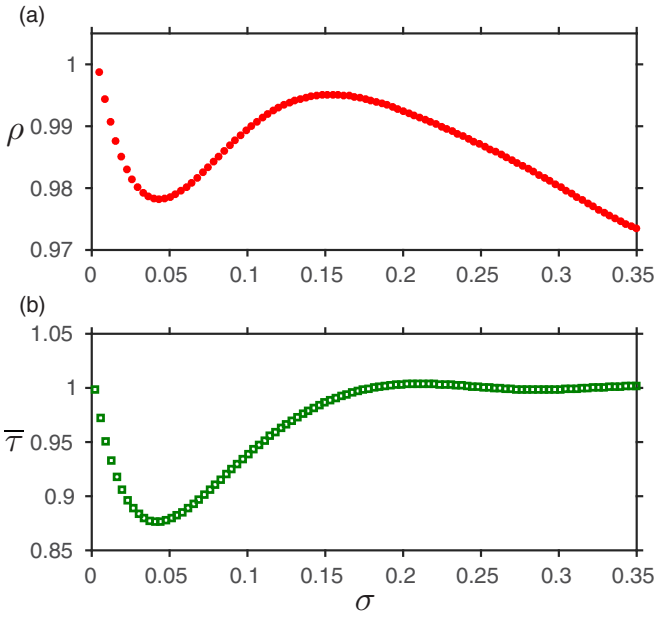

FIG. 7. Effect of periodic external force: (a) Synchrony measure (ρ) for varying standard deviation (σ) for the external force strength ($\xi = 0.005$) with fixed dispersal rate ($\epsilon = 0.6$). (b) Average period ($\overline{\tau}$) for varying σ. Here average period is rescaled to 1. Other parameters are given by $a = 1$ and $b = 1$, $r = 0.5$, $K = 0.5$, $\alpha = 1$, $\beta = 0.5$, $B = 0.16$, and $m = 0.2$.

Although in several works on spatially extended ecosystems it has been shown that multiplicative noise can induce interesting dynamics including stochastic resonance [62,63], here we choose noise in terms of randomly chosen period of oscillation. To quantify the effect of changes in σ of the heterogeneous periods of oscillation on the collective dynamics, we vary σ and we measure, for a large enough time T, a synchrony order parameter (denoted by ρ) [64], defined as

$$\rho = \sqrt{1 - \left\langle \frac{\sum_{i=1}^{N}[V_i(t) - \overline{V}(t)]^2}{\sum_{i=1}^{N} V_i(t)^2} \right\rangle} = \sqrt{\left\langle \frac{\overline{V}(t)^2}{\frac{1}{N}\sum_{i=1}^{N} V_i(t)^2} \right\rangle}, \tag{11}$$

with $\overline{V}(t) = \frac{1}{N}\sum_{i=1}^{N} V_i(t)$ and $\langle \ldots \rangle$ denoting the average over the time T. The value of the order parameter ρ varies between 0 and 1. It is equal to 0 when there is no synchrony and 1 if the patches are perfectly synchronized. The value is in between 0 and 1 when the patches are partially synchronized.

At each standard deviation σ, the synchrony measure ρ in Eq. (11) is computed for a specific external force strength $\xi = 0.005$ with the sinusoidal forcing $G(\omega t) = a + b\sin(\omega t)$ as an external force. For increasing σ, the synchrony measure ρ is shown in Fig. 7(a). We already know that without external force, they are phase synchronized due to dispersal. As far as synchrony measure is concerned, phase synchrony is denoted as a partial synchronization since the synchrony measure (ρ) is less than one. Importantly, in phase-synchronized oscillation, the amplitude varies in each patch and densities are not much correlated. However, due to the external force, species can oscillate in the same fashion and may show higher correlation. At low value of standard deviation σ, initially the synchronization measure ρ decreases; however, for increasing standard deviation, the synchrony measure improves for a range of σ values and then again declines [shown in Fig. 7(a)]. Furthermore, the average period ($\overline{\tau}$) is calculated by time averaging between the maxima of the dynamic variables. The average period is shown in Fig. 7(b). Here at low standard deviation, the average period ($\overline{\tau}$) decreases, while for higher standard deviation, the average period saturates. In spite of having higher heterogeneity in large-scale, populations are entrained by matching with external force frequency.

For a wide range of external force strength ξ, dispersal strength ϵ and variations in σ, the synchrony measure is shown using spatial diagrams in Fig. 8. In the top panel of Fig. 8, at different dispersal rates, the synchronized measure is shown in the color region for varying external force strength and standard deviation. Also, in the bottom panel of Fig. 8, at different standard deviations, this measure is shown for different values of both external force and dispersal strength. In the absence of external force $G(\omega t)$, the network of 100 patches shows either quasiperiodic oscillation or in-phase-synchronized oscillation at low dispersal rate. Once the external force is applied, the patches can behave coherently, which increases the synchrony measure. The yellow (light shaded) region in Fig. 8 shows perfect synchrony in all connected patches, whereas the dark color shaded region denotes partial synchronization. For small standard deviation, all the connected patches synchronize and show higher synchrony measure irrespective of the choice of ϵ and ξ. Important to note here that for higher σ and very low ξ, the network of 100 patches are not strongly correlated. For low σ and high ξ the synchrony improves [see Figs. 8(a)–8(d)]. Hence, there exists a trade-off between period mismatch and environmental forces which promotes synchronous as well as asynchronous dynamics. Moreover, an increase in the interaction strength ϵ further improves the correlated fluctuations for many choices of ξ and σ, which is evident from Figs. 8(a) and 8(d). Similarly, higher heterogeneity with dispersal reduces the synchrony measure at weak external force, which is noticeable from Figs. 8(e) to 8(h). Indeed, metapopulation entrainability is strongly interconnected with the combination of suitable heterogeneity, dispersal, and seasonal variations. As already mentioned, high synchrony between the patches increases the risk of global extinction during the period of depression in species density [44], and in contrast, asynchrony increases the species persistence by lowering the extinction probability [18]. Highly coherent dynamics may be dangerous for species that wish to conserve. Therefore, the obtained results can be of some interest to conservation biologists.

IV. DISCUSSION

Intrinsic heterogeneities between species residing in spatially separated habitat patches are of fundamental importance in shaping the long-term collective dynamics of spatial ecological systems [13,28,65]. At the same time, extrinsic disturbances like seasonal forcing and varying dispersal rate have strong influence on species characteristics [6,48,65]. The metapopulation model considered in this paper incorporates

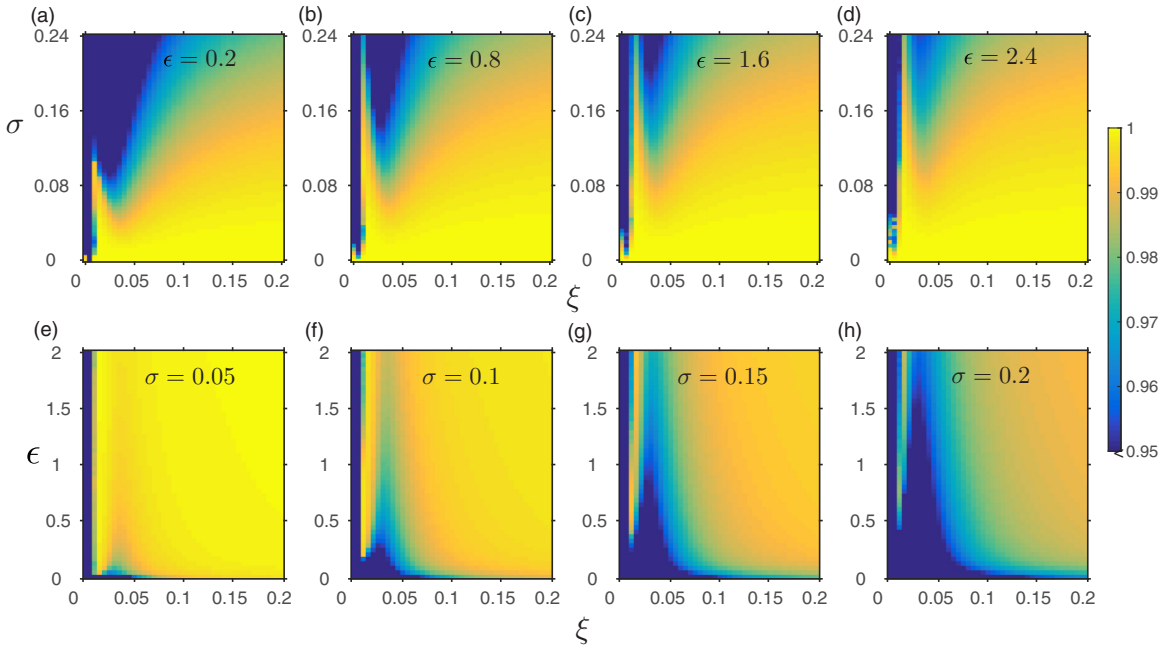

FIG. 8. Synchrony measure in a network of 100 patches: (a–d) For different dispersal rate (ϵ), the measure of synchrony is shown in the color region for continuous variation of the periodic external force strength (ξ) and standard deviation (σ) with heterogeneous periods (the top panel). Here at low σ, the network behaves coherently. However, for higher external force strength and intermediate σ, the network shows coherent behavior. (e–h) The synchrony measure for different σ is shown in the bottom panel for varying the periodic external force strength (ξ) and dispersal strength (ϵ) . Other parameters are given by $a = 0.5$ and $b = 0.5$, $r = 0.5$, $\omega = 35.76$, $K = 0.5$, $\alpha = 1$, $\beta = 0.5$, $B = 0.16$, and $m = 0.2$. See text for more details.

both the intrinsic and the extrinsic factors which could influence ecosystems and our findings highlight their importance. Explicitly, the complex dynamics of interacting species have been studied in terms of nonequilibrium state by characterizing the metapopulation model through the combination of period mismatch, dispersal, and extrinsic disturbances via seasonal forcing. We find that in the absence of seasonal forces, dispersal as a density-dependent process enables various complex dynamics, such as phase synchronization, quasiperiodicity, period-doubling of limit cycle, and even cessation of oscillation via amplitude death. Moreover, period-1 cycles and period-2 cycles through forward and reverse period-doubling bifurcations highlight the annual and multiannual cycles in metapopulation dynamics [66]. These characteristics of limit cycles from equilibrium points are distinguished by Floquet multipliers.

The sinusoidal external force resembling the extrinsic disturbances on ecological system influences all interacting species with a depression and recovery in their densities. Particularly, the plankton communities in aquatic ecosystems are often influenced by season succession which exhibits cyclic fluctuations [66–69]. Although seasonal forcing here has direct influence on resource populations, indirectly consumer populations also have been influenced by seasonal forcing due to consumer–resource interactions. While increasing synchrony among populations reduces the probability of long-term survival, it is highly necessary to understand the mechanisms behind synchronization. As the synchronized oscillations have substantial influence in community organization and persistence [8], here we have quantified the entrainment of metapopulation in two different ways using the phase-reduction approach and the correlation of temporal fluctuations. The disturbance in species density at each phase of the oscillation determines the important characteristics of seasonal forcing as well as dispersal by exhibiting higher synchrony measure in mismatch case. In addition, incorporating stochasticity in heterogeneous habitats, we have quantified the species correlated fluctuations in a rather different way using the synchrony measure. Our findings through the considered synchrony measure is important in order to understand the trade-offs between dispersal and seasonal forcing. Despite the fact that the synchrony measure is low in phase synchronization, the introduced stochasticity in heterogeneous oscillation period shows correlated fluctuations in species abundance for different external perturbations and results in a higher synchrony measure. In contrast, the on and off situations of seasonal forcing in the coupled metapopulation model enable the regular and the irregular rhythmic behavior in heterogeneous patchy environments. Our study highlights the trade-offs among dispersal, time-induced heterogeneity through period mismatch and the periodic external forcing in promoting species persistence.

Previous empirical studies have suggested that more heterogeneous landscapes support larger populations and also provide protection against extinction in a broader range of environments [70,71]. Habitat quality as an important factor in metapopulation dynamics strongly contributes to species persistence. In our study, instead of timescale separation

between species [13], the patch-wise variation detects the quality of habitat by enhancing the longevity of species. Depending on dispersal and heterogeneity level, populations are synchronized or asynchronized, leading to alter the probability of extinction and recolonization [72]. Importantly, our results are in line with previous studies on butterfly populations that higher habitat heterogeneity can promote stability and persistence [70]. Due to uniform weather conditions and year-to-year variation in extreme weather conditions, synchronizing fluctuations across the metapopulation are wide-spread [71]. However, as global persistence of metapopulation decreases for increasing correlation, our results emphasize that heterogeneity, dispersal and seasonal variation can jointly shape the metapopulation dynamics and other ecological processes. Hence, our approach provides a possible theoretical explanation in promoting synchrony as well as some control strategies in conserving species.

In summary, the combination of intrinsic and extrinsic factors influences rhythmic processes in the metapopulation model. The right balance among environmental heterogeneity, dispersal and seasonal forcing show various synchronous behavior. Our study focuses on the appropriate environmental heterogeneity and dispersal in conserving species from habitat loss. Though stochastic variations have been used indirectly in habitat heterogeneity, further investigations are needed with presence of additive and multiplicative noise as well as higher trophic interactions. Further, instead of simple diffusive coupling in dispersal, global connection also can enhance the heterogeneous spatial ecosystem properties. Subsequently, instead of introducing heterogeneity in timescale of entire patch, if we use distinct timescale in each species (i.e., slow-fast systems), then resulting dynamics could even be more interesting. Moreover, the seasonal force can also be incorporated in the model in other ways [8], such as in the growth rate and/or in the mortality rate.

ACKNOWLEDGMENTS

We convey our sincere thanks to the anonymous referees for insightful comments. P.S.D. acknowledges the financial support from SERB, Department of Science and Technology (DST), India (Grant No. YSS/2014/000057).

APPENDIX: FLOQUET MULTIPLIERS

Qualitative dynamics of the oscillating system can be analyzed using Floquet theory. In the absence of external force, the diffusive coupled system shows nonequilibrium dynamics through oscillatory behavior. Since the stability of nonequilibrium state is difficult to analyze mathematically, Floquet theory has been used to test the stability of the limit cycle [42]. In particular, from the considered system, the Floquet multipliers are calculated numerically using matrix

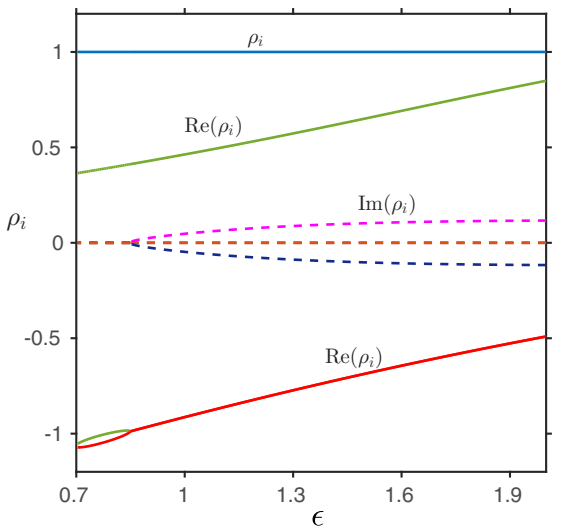

FIG. 9. Floquet multipliers: For continuous variation of the dispersal rate (ϵ) in the system [Eq. (1)], all the Floquet multipliers (ρ_i) with it's real part (solid lines) and imaginary parts (dotted lines) are shown. All the other parameters are the same as described in the caption of Fig. 3(b).

differential equations in terms of the $m\times 1$ matrix $Q(t)$:

$$\frac{dQ(t)}{dt} = DF(\mathbf{z}_0(t))Q(t). \tag{A1}$$

Here $DF(\mathbf{z}_0)$ is a periodic function with period τ in a stable orbit $\mathbf{z}_0$. By integrating Eq. (A1) numerically over a period τ with an identity matrix as an initial condition, we get the Floquet solutions, which is denoted by

$$Q(t) = \sum_{i=1}^{m} c_i \exp(\mu_i t)\mathbf{v}_i(t), \tag{A2}$$

where μ_i's are the Floquet or characteristic exponents, $\mathbf{v}_i$'s are vector-valued functions with period τ, and c_i is a coefficient determined by initial conditions. The relationship between the Floquet exponents and the period (τ) is given as the Floquet multipliers (ρ_i) by $\rho_i = \exp(\mu_i \tau)$. The Floquet multipliers are obtained as the eigenvalues of the matrix $Q(t = T)$ and hence m-dimensional system has m Floquet multipliers. Based on Floquet multipliers, the stability of limit cycle can be identified. In the considered system Eq. (1), one of the multipliers $\rho_i = 1$ represents pure phase shift in limit cycle. The torus bifurcation of limit cycle is identified when ρ_i pass through the unit circle $|\rho| = 1$ on the complex plane. Also period-doubling bifurcation of the limit cycle can be identified if a single real Floquet multiplier passes through -1. In Fig. 9, we have shown the Floquet multipliers of the system [Eq. (1)] for varying dispersal rate (ϵ). Indeed, the phase synchronization and the period doubling of the limit cycles of Fig. 3(b) are identified by the Floquet multipliers.

[1] L. Glass and M. C. Mackey, *From Clocks to Chaos: The Rhythms of Life* (Princeton University Press, New Jersey, 1988).
[2] A. Goldbeter, Nature **420**, 238 (2002)
[3] D. Gonze, S. Bernard, C. Waltermann, A. Kramer, and H. Herzel, Biophys. J. **89**, 120 (2005).
[4] U. Sommer, BioScience **35**, 351 (1985).

[5] L. Glass, Nature **410**, 277 (2001).
[6] E. Ranta, V. Kaitala, J. Lindstrom, and H. Linden, Proc. R. Soc. London B **262**, 113 (1995).
[7] G. F. Fussmann, S. P. Ellner, K. W. Shertzer, and N. G. J. Hairston, Science **290**, 1358 (2000).
[8] S. P. Ellner and G. Fussmann, Ecology **84**, 882 (2003).
[9] J. E. Keymer, P. A. Marquet, J. X. Velasco-Hernandez, and S. A. Levin, Am. Nat. **156**, 478 (2000).
[10] I. Hanski, Nature **396**, 41 (1998).
[11] C. J. Briggs and M. F. Hoopes, Theoret. Pop. Biol. **65**, 299 (2004).
[12] E. E. Goldwyn and A. Hastings, Theoret. Pop. Biol. **73**, 395 (2008).
[13] E. E. Goldwyn and A. Hastings, Bull. Math. Biol. **71**, 130 (2009).
[14] I. Hanski, *Metapopulation Ecology* (Oxford University Press, Oxford, 1999).
[15] I. A. Hanski, Proc. Natl. Acad. Sci. USA **108**, 14397 (2011).
[16] E. Ranta, V. Kaitala, and J. Lindstrom, Proc. R. Soc. London B **266**, 1851 (1999).
[17] A. Hastings and L. Gross, *Encyclopedia of Theoretical Ecology* (University of California Press, Berkeley, 2012).
[18] M. D. Holland and A. Hastings, Nature **456**, 792 (2008).
[19] V. A. A. Jansen, Theoret. Pop. Biol. **59**, 119 (2001).
[20] T. Banerjee, P. S. Dutta, and A. Gupta, Phys. Rev. E **91**, 052919 (2015).
[21] T. Banerjee, P. S. Dutta, A. Zakharova, and E. Schöll, Phys. Rev. E **94**, 032206 (2016)
[22] A. Gupta, T. Banerjee, and P. S. Dutta, Phys. Rev. E **96**, 042202 (2017)
[23] B. Cazelles and G. Boudjema, Am. Nat. **157**, 670 (2001).
[24] A. J. Allstadt, A. M. Liebhold, D. M. Johnson, R. E. Davis, and K. J. Haynes, Ecology **96**, 2935 (2015).
[25] T. M. Massie, B. Blasius, G. Weithoff, U. Gaedke, and G. F. Fussmann, Proc. Natl. Acad. Sci. USA **107**, 4236 (2010).
[26] E. Post and M. C. Forchhammer, Proc. Natl. Acad. Sci. USA **101**, 9286 (2004).
[27] L. Fahrig, Ann. Rev. Ecol. Evol. Systemat. **34**, 487 (2003)
[28] A. Liebhold, W. D. Koenig, and O. N. Bjørnstad, Ann. Rev. Ecol. Evol. Systemat. **35**, 467 (2004)
[29] P. Amarasekare, Ann. Rev. Ecol. Evol. Systemat. **39**, 479 (2008)
[30] A. Stein, K. Gerstner, and H. Kreft, Ecol. Lett. **17**, 866 (2014)
[31] A. Koseska, E. Volkov, and J. Kurths, Phys. Rep. **531**, 173 (2013).
[32] R. Muneepeerakul, S. Azaele, S. A. Levin, A. Rinaldo, and I. Rodriguez-Iturbe, J. Theor. Biol. **269**, 256 (2011).
[33] F. Guichard, S. A. Levin, A. Hastings, and D. Siegel, BioScience **54**, 1003 (2004).
[34] R. Arumugam, P. S. Dutta, and T. Banerjee, Phys. Rev. E **94**, 022206 (2016)
[35] Y. Kuramoto, *Chemical Oscillations, Waves, and Turbulence* (Springer, New York, 1984).
[36] P. F. Pinsky and J. Rinzel, Biol. Cybernet. **73**, 129 (1995).
[37] M. L. Rosenzweig and R. H. MacArthur, Am. Nat. **97**, 209 (1963).
[38] C. A. Johnson and P. Amarasekare, Am. Nat. **185**, 87 (2015).
[39] S. Dey, S. Dabholkar, and A. Joshi, J. Theor. Biol. **238**, 78 (2006).
[40] A. Pikovsky, M. Rosenblum, and J. Kurths, *Synchronization: A Universal Concept in Nonlinear Sciences* (Cambridge University Press, Cambridge, UK, 2003).
[41] M. Candaten and S. Rinaldi, Theoret. Pop. Biol. **63**, 257 (2003).
[42] C. A. Klausmeier, Theoret. Ecol. **1**, 153 (2008)
[43] B. Blasius, A. Huppert, and L. Stone, Nature **399**, 354 (1999).
[44] D. J. D. Earn, S. A. Levin, and P. Rohani, Science **290**, 1360 (2000).
[45] Q. X. Liu, Z. Jin, and B. L. Li, J. Stat. Mech. (2008) P05011.
[46] C. Fontaine and A. Gonzalez, Ecology **86**, 1463 (2005).
[47] D. A. Vasseur and J. W. Fox, Nature **460**, 1007 (2009).
[48] E. Ranta, V. Kaitala, J. Lindstrom, and E. Helle, Oikos **78**, 136 (1997).
[49] J. Ripa, Oikos **89**, 175 (2000).
[50] S. Altizer, A. Dobson, P. Hosseini, P. Hudson, M. Pascual, and P. Rohani, Ecol. Lett. **9**, 467 (2006)
[51] T. P. Turchin and I. Hanski, Am. Nat. **149**, 842 (1997).
[52] R. A. Taylor, A. White, and J. A. Sherratt, J. Theor. Biol. **365**, 55 (2015).
[53] R. M. Smeal, G. B. Ermentrout, and J. A. White, Philos. Trans. R. Soc. Lond. B. Biol. Sci. **365**, 2407 (2010).
[54] E. M. Izhikevich, *Dynamical Systems in Neuroscience: The Geometry of Excitability and Bursting* (MIT Press, Cambridge, MA, 2008).
[55] V. Novičenko and K. Pyragas, Nonlin. Dynam. **67**, 517 (2012).
[56] Y. Hasegawa and M. Arita, J. R. Soc. Interface **10**, 20121020 (2013)
[57] V. Dakos, E. Benincà, E. H. van Nes, C. J. M. Philippart, M. Scheffer, and J. Huisman, Proc. R. Soc. B **276**, 2871 (2009).
[58] S. Gubbins and C. A. Gilligan, Proc. R. Soc. London B **264**, 227 (1997).
[59] A. Bohn and J. García-Ojalvo Massie, J. Theor. Biol. **250**, 37 (2008).
[60] T. M. Massie, G. Withoff, N. Kuckländer, U. Gaedke, and B. Blasius, Nat. Commun. **6**, 5993 (2015)
[61] J. W. Fox, G. Legault, D. A. Vasseur, and J. A. Einarson, PLoS ONE **8**, e79527 (2013)
[62] D. Valenti, A. Fiasconaro, and B. Spagnolo, Acta Phys. Pol. B **35**, 1481 (2004).
[63] A. Fiasconaro, D. Valenti, and B. Spagnolo, Acta Phys. Pol. B **35**, 1491 (2004).
[64] N. Komin, A. C. Murza, E. Hernandez-Garcia, and R. Toral, Interface Focus **1**, 167 (2011)
[65] E. E. Goldwyn and A. Hastings, J. Theor. Biol. **289**, 237 (2011).
[66] C. A. Klausmeier, J. Theor. Biol. **262**, 584 (2010).
[67] U. Sommer, R. Adrian, L. D. S. Domis, J. J. Elser, U. Gaedke, B. Ibelings, E. Jeppesen, M. Lürling, J. C. Molinero, W. M. Mooij, E. V. Donk, and M. Winder, Ann. Rev. Ecol. Evol. Systemat. **43**, 429 (2012)
[68] G. Denaro, D. Valenti, B. Spagnolo, G. Basilone, S. Mazzola, S. W. Zgozi, S. Aronica, and A. Bonanno, PLoS ONE **8**, e66765 (2013)
[69] D. Valenti, G. Denaro, R. Ferreri, S. Genovese, S. Aronica, S. Mazzola, A. Bonanno, G. Basilone, and B. Spagnolo, Sci. Rep. **7**, 220 (2017)
[70] T. Oliver, D. B. Roy, J. K. Hill, T. Brereton, and C. D. Thomas, Ecol. Lett. **13**, 473 (2010)
[71] A. J. M. Tack, T. Mononen, and I. Hanski, Proc. R. Soc. London B **282**, 20150173 (2015).
[72] C. F. Steiner, R. D. Stockwell, V. Kalaimani, and Z. Aqel, Oikos **122**, 1195 (2013).